Modeling Simulation and Experimental Study on Valveless Electro-Hydraulic Servo Steering Device for Ship

Jian Liao [1,2,a],Lin He [1,2,a] Rongwu Xu [1,2,b,*],Zongbin Chen[1,2,a]

1.Institute of Noise&Vibration, Naval University of Engineering Wuhan 430033,China;

2.State Key Laboratory of Ship Vibration&Noise, Wuhan 430033,China

[a] jl_zss@sina.com

[b]rw_zss@163.com

Corresponding Author：Rongwu Xu

Keywords: Valveless electro-hydraulic servo steering device, Nonlinear, AMESim, Static characteristics, Dynamic characteristics

Abstract. The linear model of valveless electro-hydraulic servo steering device neglects the nonlinear factors, especially the factors of the control subsystem, so the quantitative static and dynamic characteristics of the actual system cannot be evaluated accurately. Aiming at the problem, the steering device for a certain ship is chosen as the studying object and the nonlinear mathematical models of the control subsystem and hydraulic transmission subsystem are derived by a full consideration of the nonlinear factors and the linear factors which are not considered in the linear model. Utilizing the coupling relationship between two subsystems, the nonlinear simulation model is set up in AMESim. By simulation analysis and experimental verification, it is proved that the nonlinear mathematical model in this paper can evaluate the static and dynamic characteristics more accurately, which is of great significance to the design and optimization of the valveless electro-hydraulic servo steering device.

1. Introduction

Due to the serious control valve's throttling loss (such as the valve-controlled steering device) and continuous high speed operation of motor (such as pump-controlled steering device), the traditional electro-hydraulic servo steering device has the great throttling noise and air noise as well as the large power loss, which limits its application in many fields, especially in the low noise field [1-3]. The valveless electro-hydraulic servo steering device (VSSD for short) operates in the direct drive working principle, which adjusts its output flow by changing the motor speed, instead of the pump displacement or control valve's opening, to achieve the velocity and position control [4]. As the control valve's throttling loss is eliminated and the continuous high speed operation of motor is avoided, the VSSD has the advantages of high efficiency, low noise and high reliability. Consequently, the VSSD is being widely used in the civil and military fields in the replace of the traditional electro-hydraulic servo steering device [5-8].

The purpose of modeling and simulation is to quantitatively evaluate the static and dynamic characteristics as well as instruct the design and optimization [9,10]. Currently, it is popular to deduce the VSSD's mathematical models by the linear method, and then evaluate the static and dynamic characteristics based on this model. This method can simulate the influence of relative parameters on the static and dynamic characteristics qualitatively [11-14]. However, as it neglects the nonlinear factors and the linear factors that is not considered by the typical linear method (such as the time lag result from the sampling time, the parameters of the controller variable with the speed, etc.), the linear mathematical model cannot assess the VSSD's quantitative static and dynamic characteristics accurately. In addition, the VSSD's operational condition is external load-dependent. As the VSSD's actual operational condition deviates from the interest point of linear mathematical model largely, the simulation results would greatly differ from the actual ones, causing that the VSSD's actual static and dynamic characteristics cannot meet the requirements.

The VSSD for a certain ship is chosen as the studying object, and deduce its nonlinear mathematical model. Then, the static and dynamic characteristics is evaluated based on the simulation model set up in AMESim software [15,16]. Finally, the correctness and accuracy of the nonlinear mathematical model in this paper is verified by experiments.

2. Modeling of the VSSD

The VSSD mainly consists of two parts: the hydraulic transmission subsystem and the control subsystem. As is shown in Fig.1, the hydraulic transmission subsystem contains a AC permanent magnet synchronous motor, a bi-directional quantitative pump and a hydraulic cylinder while the control subsystem is mainly made up of a controller, a servo drive and a sensor group. The VSSD's working principle is that the AC permanent magnet synchronous motor which works as not only a driving source but also a control component, drives the bi-directional quantitative pump, and the hydraulic cylinder can run to a specified position with a certain velocity by the pump's outlet flow. Meanwhile, the pressure, position, velocity and other state parameters would be fed back to the controller by the sensor group for the timely adjustment of the rotary speed and torque of AC permanent magnet synchronous motor, which can achieves the high-accuracy position and velocity control.

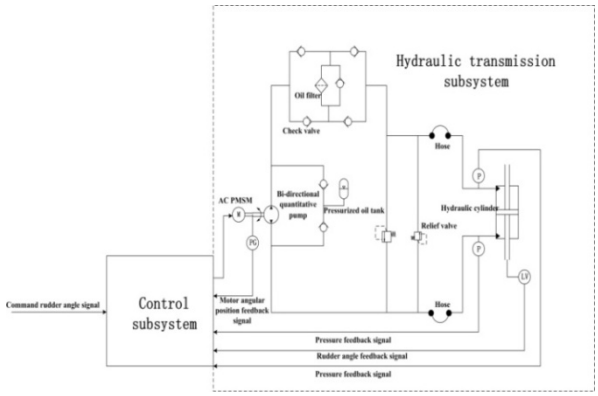

Fig.1. VSSD's components diagrams

In this section, the nonlinear mathematical models of control subsystem and hydraulic transmission subsystem are deduced. Then, the simulation model is set up in AMESim by consideration of the coupling relationship between two subsystems.

2.1 Mathematical model of the control subsystem

The control subsystem adopts the servo control principle based on magnetic field orientation. In Fig.2, there are three closed loops, which are the position loop, speed loop and current loop from outside to inside. The working process is that firstly, the command rudder angle signal subtracts the feedback angle signal from the hydraulic transmission subsystem to obtain the rudder angle error signal which generates the target speed through the position controller. Then, the speed error signal is obtained with the target speed signal subtracting the motor's actual speed, by which the target quadrature axis current is produced through the speed controller. Finally, the target quadrature axis current signal subtracts the actual quadrature axis current to generate the current error signal, which goes through the current controller, PWM signal control unit and power inverter for the production of the corresponding stator current. The stator current is channeled to the servo motor to generate torque which drives the hydraulic transmission subsystem.

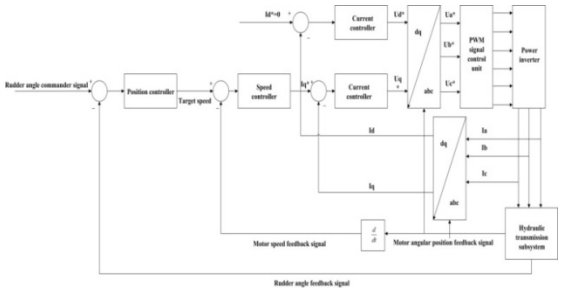

Fig.2. Schematic diagram of the control subsystem

Digital incremental PI control algorithm is applied to the position controller, speed controller and current controller. The target speed is adjusted through the position controller according to the rudder angle error :

$$\begin{aligned}
&\Delta\omega^*(kt_1) = k_{p1}(e_\Theta(kt_1) - e_\Theta((k-1)t_1)) + k_{i1}e_\Theta(kt_1)\\
&a(kt_1) = \frac{\Delta\omega^*(kt_1)}{t_1}\\
&\omega^*(kt_1) = \begin{cases}\omega^*((k-1)t_1) + \Delta\omega^*(kt_1), a(kt_1) < a_{\max}\\ \omega^*((k-1)t_1) + a_{\max}t_1, a(kt_1) \ge a_{\max}\end{cases}
\end{aligned} \tag{1}$$

Where $\omega^*(kt_1)$ is the target speed signal produced in the kth time sampling. t_1 denotes the sampling time of the position controller. $e_\Theta(kt_1)$ and $a(kt_1)$ are the rudder angle error signal and the speed changing rate in the kth time sampling respectively. $a_{\max}$ is the maximum setting changing rate of the motor speed.

Based on the input speed error, the speed controller outputs the corresponding target quadrature axis current:

$$\begin{aligned}
&\Delta i_q^*(kt_2) = k_{p2}(e_n(kt_2) - e_n((k-1)t_2)) + \frac{k_{p2}}{T_{n2}}e_n(kt_2)\\
&i_q^*(kt_2) = i_q^*((k-1)t_2) + \Delta i_q^*(kt_2)\\
&k_{p2} = \begin{cases}K_{p20}, |n(kt_2)| \le 1112.5\\ -\dfrac{0.506K_{p20}}{3337.5}(|n(kt_2)| - 1112.5) + K_{p20}, 1112.5 < |n(kt_2)| \le 4450\\ 0.494K_{p20}, |n(kt_2)| > 4450\end{cases}\\
&T_{n2} = \begin{cases}T_{n20,}, |n(kt_2)| \le 1112.5\\ \dfrac{3T_{n20}}{3337.5}(|n(kt_2)| - 1112.5) + T_{n20}, 1112.5 < |n(kt_2)| \le 4450\\ 4T_{n20}, |n(kt_2)| > 4450\end{cases}
\end{aligned} \tag{2}$$

Where $i_q^*(kt_2)$ denotes the target quadrature axis current produced in the kth time sampling. t_2 is the sampling time of speed controller. $e_n(kt_2)$ is the speed error signal in the kth time sampling. $n(kt_2)$ is the rotary speed of motor in the kth time sampling. k_{p2} and T_{n2} are the proportional coefficient and the integratal time respectively which vary with the rotary speed of motor $n(kt_2)$.

Quadrature axis current and direct axis current are transmitted into their current controller to produce the quadrature axis voltage and direct axis voltage respectively:

$$\begin{aligned}
&\Delta u_d^*(kt_3) = k_{p3}(e_{id}(kt_3) - e_{id}((k-1)t_3)) + \frac{k_{p3}}{T_{n30}}e_{id}(kt_3)\\
&\Delta u_q^*(kt_3) = k_{p3}(e_{iq}(kt_3) - e_{iq}((k-1)t_3)) + \frac{k_{p3}}{T_{n30}}e_{iq}(kt_3)\\
&u_d^*(kt_3) = u_d^*((k-1)t_3) + \Delta u_d^*(kt_3)\\
&u_q^*(kt_3) = u_q^*((k-1)t_3) + \Delta u_q^*(kt_3)\\
&k_{p3} = \begin{cases}K_{p30}, |i_q(kt_3)| \le 13.27\\ -\dfrac{0.59K_{p30}}{110.73}(|i_q(kt_3)| - 13.27) + K_{p30}, 13.27 < |i_q(kt_3)| \le 124\\ 0.41K_{p30}, |i_q(kt_3)| > 124\end{cases}
\end{aligned} \tag{3}$$

Where $u_q^*(kt_3)$ and $u_d^*(kt_3)$ are the target quadrature axis voltage signal and direct axis voltage

signal produced in the kth time sampling respectively. t_3 is the sampling time of the current controller. $e_{iq}(kt_3)$ and $e_{id}(kt_3)$ denote the quadrature axis current error signal and direct axis current error signal in the kth time sampling respectively. k_{p3} is the proportional coefficient which varies with the quadrature axis current $i_q(kt_3)$ and T_{n30} is the integratal time constant.

The conversion from the rotor voltages to the stator voltages, namely u_q^*, u_d^* to u_a^*, u_b^*, u_c^*, is performed by Park inverse transformation and Clark inverse transformation [17].

$$\begin{bmatrix} u_a^*(kt_3) \\ u_b^*(kt_3) \\ u_c^*(kt_3) \end{bmatrix} = \sqrt{\frac{2}{3}} \begin{bmatrix} \cos\theta(kt_3) & -\sin\theta(kt_3) \\ \cos(\theta(kt_3) - \frac{2\pi}{3}) & -\sin(\theta(kt_3) - \frac{2\pi}{3}) \\ \cos(\theta(kt_3) + \frac{2\pi}{3}) & -\sin(\theta(kt_3) + \frac{2\pi}{3}) \end{bmatrix} \begin{bmatrix} u_d^*(kt_3) \\ u_q^*(kt_3) \end{bmatrix} \tag{4}$$

After passing through the PWM controller unit and power inverter, the stator voltages u_a^*, u_b^*, u_c^*, produce three-phase pulse voltages which stimulate rotary magnetic field in the stator winding of AC permanent magnet synchronous motor to drive the motor [18,19]. Consequently, Eqs. (1)-(4) represent the nonlinear mathematical model of the control subsystem.

2.2 Mathematical model of the hydraulic transmission subsystem

As the input of the hydraulic transmission subsystem, three-phase pulse voltages of the stator winding generate the corresponding three-phase currents i_a, i_b, i_c which are used for the generation of the torque of motor:

$$\begin{aligned} T_d &= p_m \Psi^r i_s \\ i_s &= i_a + i_b e^{j\frac{2\pi}{3}} + i_c e^{-j\frac{2\pi}{3}} \end{aligned} \tag{5}$$

Where T_d is the driving torque of the motor. p_m is the pole pairs of the motor. Ψ^r and i_s denote the permanent magnet flux linkage and the synthetic stator current respectively.

The shafts of the AC permanent magnet motor and hydraulic pump which constitute the VSSD's power unit, are connected by an elastic coupling. According to the Newton's second law, the dynamic equations of the power unit are obtained:

$$T_d - T_L = J\frac{d\omega}{dt} + B_\omega \omega \tag{6}$$

Where T_L is the output torque of the power unit. J is the moment of inertia. B_ω is the viscosity coefficient. ω is the actual angle speed of the motor.

The flow is discharged as the power unit operates. On the basis of the flow continuity of the power unit, the flow equations are obtained as follows:

$$\begin{aligned} Q_f &= nD - C_{ep}P_e - C_{ip}(P_e - P_i) \\ n &= \omega / 2\pi \end{aligned} \tag{7}$$

Where Q_f is the output flow of the power unit. D is the hydraulic pump displacement. P_e is the outlet pressure of the hydraulic pump. P_i is the inlet pressure of the hydraulic pump. C_{ep} is the external leakage coefficient of the hydraulic pump. C_{ip} is the internal leakage coefficient of the hydraulic pump.

Owing to the integrated design of the VSSD's hydraulic oil source, the pipe is short. For this reason, the pipe flow continuity equations can be derived by the lumped parameter method:

$$\begin{aligned} Q_{in} - Q_{out} &= \frac{A_p L_p}{\beta_e}\frac{dP}{dt} \\ Q_{in} &= Q_f \end{aligned} \tag{8}$$

Where Q_{in} is the pipe input flow. Q_{out} is the pipe output flow. A_p is the pipe cross-sectional area. L_p is the pipe length. β_e is the effective bulk modulus of the hydraulic oil.

The output flow of the power unit is transported to the hydraulic cylinder through the pipe and then drive the cylinder. The following equations are obtained according to the cylinder flow continuity and force equilibrium:

$$
\begin{aligned}
&Q_{out} = A_a \frac{dx}{dt} + \frac{V}{\beta_e}\frac{dP}{dt} + C_{tm}P \\
&(P - P_i)A = m\frac{dx^2}{dt^2} + B_v\frac{dx}{dt} + B_a(\frac{dx}{dt})^2 + K_1 x + F_f + F_L \\
&F_f = \begin{cases} F_c sign(\dot{x}), \dot{x} \neq 0 \\ F_s, \qquad\quad \dot{x} = 0 \end{cases} \\
&\Theta = k_2 x \\
&F_L \approx k_3 \cdot \Theta \\
&sign(\dot{x}) = \begin{cases} +1, \dot{x} > 0 \\ -1, \dot{x} < 0 \end{cases}
\end{aligned}
\tag{9}
$$

Where A_a is the action area of the hydraulic cylinder. V is the controlled chamber volume of the hydraulic cylinder. x is the output displacement of the hydraulic cylinder. θ is the VSSD's output rudder angle. C_{tm} is the total leakage coefficient of the hydraulic cylinder. m is the total mass of the hydraulic cylinder and load. B_a and B_v are the windage coefficient and velocity viscosity coefficient of the hydraulic cylinder respectively. F_c, F_s and F_L denote the Coulomb friction force, the static friction and the external load respectively. K_1、k_2 and k_3 are the elastic load stiffness, the conversion coefficient between rudder angle and displacement, the conversion coefficient between external force and rudder angle respectively.

Obviously, Eqs. (5)-(9) represent the nonlinear mathematical model of the hydraulic transmission subsystem.

2.3 Simulation model of the VSSD

Based on the VSSD's operating principle and the nonlinear mathematical models of two subsystems above, the VSSD's simulation model in Fig.3 is set up in AMESim by a full consideration of the coupling relationship between two subsystems. Both the driving torque of the motor T_d and the output displacement of the hydraulic cylinder x are the coupling parameters of two subsystems which are the output of one subsystem as well as the input of the other subsystem.

Lacking of the hydraulic pump module with consideration of the leakage in AMESim, the model in Fig.4 is used to represent it, among which throttle valve A and the shuttle valve B simulate the internal leakage and external leakage of the hydraulic pump respectively.

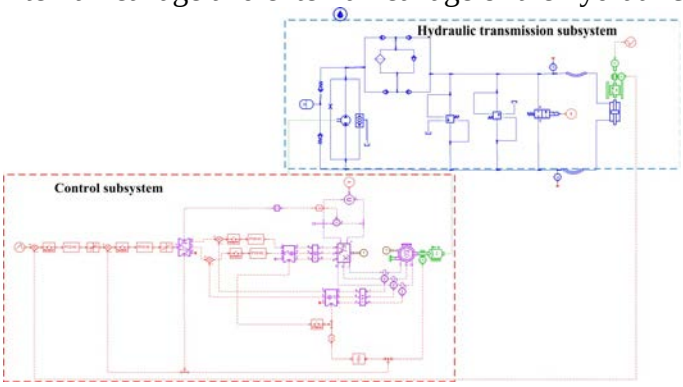

Fig.3. VSSD's simulation model in AMESim

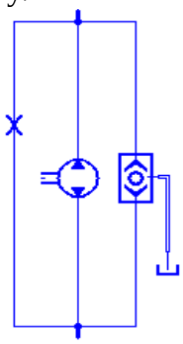

Fig.4. Pump model with consideration of the leakage

As is shown in the VSSD's nonlinear mathematical model and simulation model above, the nonlinear factors are the parameters of the controllers k_{p2}, T_{n2} and k_{p3} as well as the static friction F_s and coulomb friction force F_c of the hydraulic transmission subsystem. In addition, the sampling time t_1、t_2、t_3 and the maximum setting changing rate of the motor speed $a_{\max}$ is also considered. Those are the key factors for the accurate quantitative evaluation of the VSSD's static and dynamic characteristics.

3. Simulation analysis

The VSSD's linear simulation model in Fig.5 is set up by the method of reference [20].The function of parameters in the linear simulation model can be obtained by the Ref. [20].

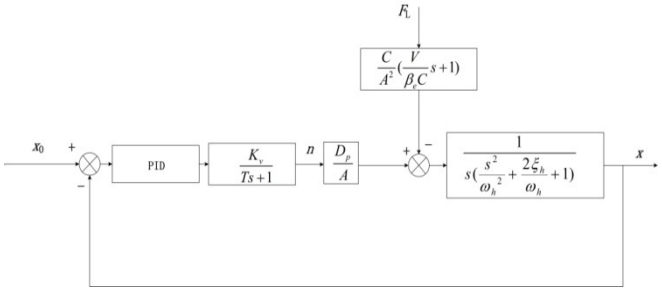

Fig.5. Linear simulation model of the VSSD

The VSSD's static and dynamic characteristics are evaluated based on two models in Fig.3 and Fig.5 respectively, then compare simulation results from them. The main simulation parameters are listed in Table 1.

Table 1 Value of the main simulation parameters

Parameter	Value	Unit
t_1	0.1	s
k_{p1}	100	rad/deg
k_{i1}	0.02	s
t_2	1.25×10^{-7}	s
K_{p20}	0.5	Nm/rad
T_{n20}	7.28×10^{-3}	s
t_3	1.25×10^{-7}	s
K_{p30}	15.367	A/Nm
T_{n30}	0.002	s
ρ	860	kg/m^3
β	6000	bar
A	0.0672	m^2
A_p	8.04×10^{-4}	m^2
V	0.043	m^3
C_{tm}	4.97×10^{-10}	$m^3/s/Pa$
C_{tp}	9.13×10^{-10}	$m^3/s/Pa$
D	63	mL/r
M	250	kg
B_v	150	N/m/s
B_a	1000	$N/(m/s)^2$
B_ω	0.0406	Nm/(rad/s)
k_2	155.6	deg/m
k_3	3428.6	N/deg

3.1 Simulation analysis of step response

Input the step rudder angle signal with amplitude value of +15°into two models, and monitor the output speed of the motor and the output rudder angle. The results are shown in Fig. 6 and 7.

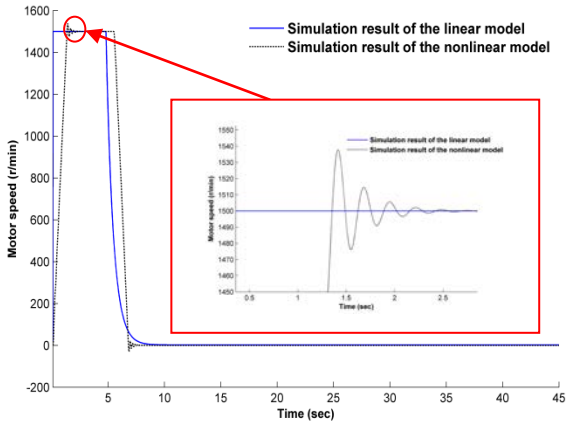

Fig.6. Simulation results of motor speed

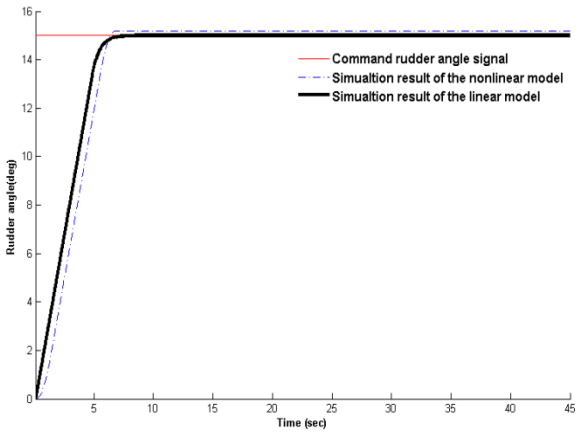

Fig.7. Simulation results of rudder angle

Fig.7 shows that the rudder angle output trend of the nonlinear model is consistent with that of the linear model, which has no overshoot neither. However, the adjustment time ts and static error E of the output rudder angle are different with each other. Table 2 further demonstrates that the adjustment time ts of the linear model is shorter than those of the nonlinear model and static error of the linear model is also smaller, which indicates the static and dynamic characteristics simulated from the linear model is superior to those simulated from the nonlinear model. In Fig.6, the great differences between the linear model and nonlinear model existing in the stage of acceleration and deceleration originate from two aspects:

(1) The motor model is simplified to the first order model without the consideration of the setting changing rate of the motor speed $a_{\max}$. In the stage of acceleration and deceleration, the motor of the linear model operates with the maximum speed changing rate (the maximum is determined by the time constant in the first order model), which results in the less adjustment time than that of nonlinear model.

(2) The parameters of the controllers in the nonlinear model k_{p2}, T_{n2} and k_{p3} vary with the speed of the motor n and the quadrature axis current i_q respectively, which results in the overshoot of the speed in the acceleration and deceleration stage. However, the parameters of the PID controller in the linear model are constant, which cause no overshoot.

Table 2 Simulation results of the VSSD's static and dynamic characteristics

	Value of t_s	**Value of E**
Nonlinear Model	5.89s	-0.19°
Linear Model	5.3s	+0.01°

3.2 Simulation analysis of system bandwidth

The system bandwidth is one of the VSSD's important performance indexes, which represents the VSSD's ability of following the command signal and restraining the disturbance signal [21]. The system bandwidth ω_b of the linear model can be obtained by Bode diagram in Fig.8.

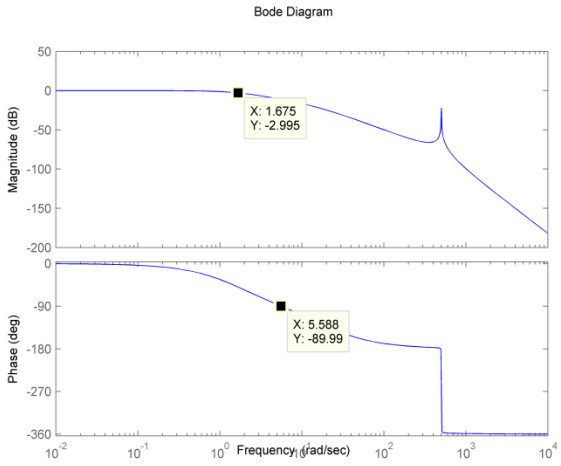

Fig.8. Bode diagram of the linear model

In Fig.8, the amplitude angular frequency ω_1 is equivalent to 1.675rad/s when the amplitude attenuation is lower than -3dB, and the phase angular frequency ω_2 equals to 5.588rad/s under the phase lag is less than -90°. The VSSD's system bandwidth evaluated from the simulation model is 0.27Hz according to eq. (10) .The reason why the VSSD can't follow the input command signal is the excessive amplitude attenuation.

$$\omega_b = \min(\omega_1, \omega_2) / 2\pi \qquad (10)$$

Because of the nonlinear factors, it's infeasible to calculate the VSSD's system bandwidth by drawing Bode diagram of simulation model in Fig.3. An alternative method, that is comparing the input sine rudder angle signals of different frequencies and small amplitude (the amplitude value is 2° in this section) with the corresponding output rudder angle signal, is used for the calculation of the VSSD's system bandwidth of the simulation model in Fig.3. The results are shown in Fig.9 and 10， which is that the VSSD's system bandwidth is 0.18Hz by this method, and the overlarge phase lag is the reason why the VSSD can't follow the input command signal.

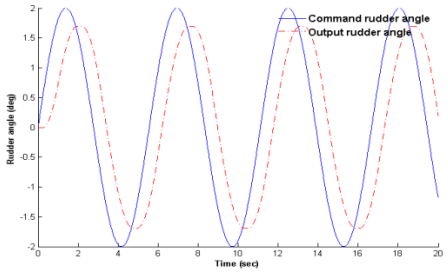

Fig.9. Simulation results of the sine rudder angle signal with frequency value of 0.18Hz

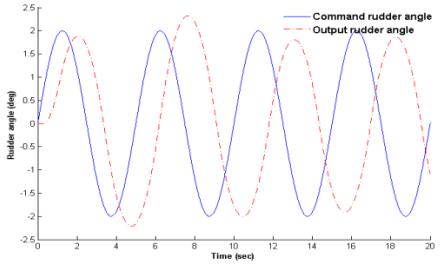

Fig.10. Simulation results of the sine rudder angle signal with frequency value of 0.2Hz

4. Experimental verification

In order to verify the accuracy of the nonlinear model, the step response experiment and system bandwidth experiment are conducted on the prototype in Fig.11.

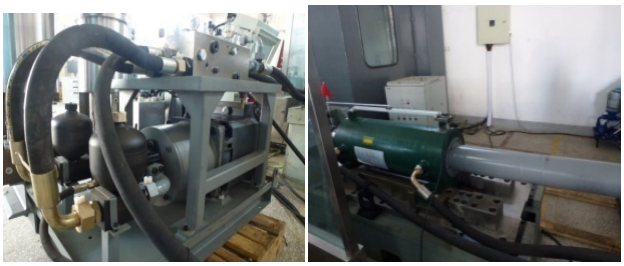

Fig.11. VSSD's prototype for experiment

4.1 Step response experiment

The step rudder angle signal with the amplitude value of +15°is input into the experimental device. Both the output rudder angle signal and the motor speed signal are measured, which are also compared with the corresponding simulation results above.

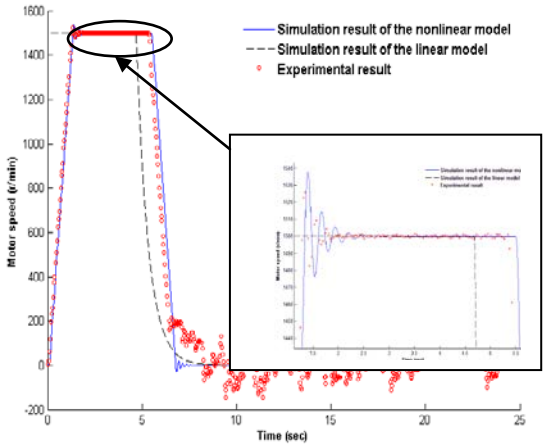

Fig.12. Contrasting results of the motor speed

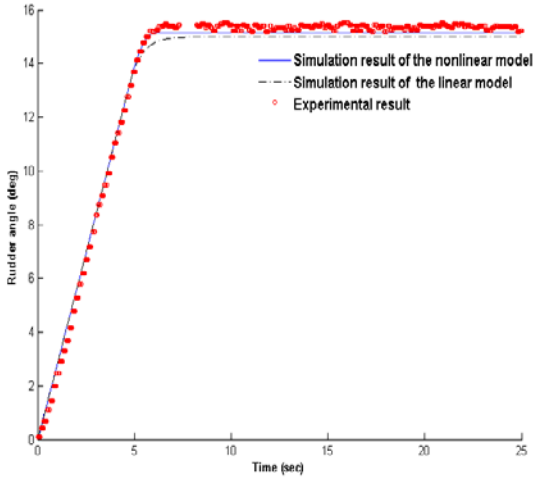

Fig.13. Contrasting results of the rudder angle

As is shown in Fig.12 and 13, the nonlinear model can assess the VSSD's actual performance more accurately compared with the linear model, which is further demonstrated by the quantitative static and dynamic characteristics from Table 3. The reason is that the nonlinear model contains the factors (such as the sampling time, the coulomb friction force, etc.) that are key to the accurate quantitative evaluation of the VSSD's static and dynamic characteristics. For example, the dynamic performance degrades as the sampling time increases and the static performance degrades with the dead zone resulted from the coulomb friction force.

Table3 Contrasting results of the VSSD's static and dynamic characteristics

	Value of t_s	**Value of E**
Nonlinear Model	5.89s	-0.19°
Linear Model	5.3s	+0.01°
Experiment	5.9s	-0.23°

4.2 System bandwidth experiment

Input the sine rudder angle signals with the amplitude value of 2°, frequencies of 0.18Hz and 0.2Hz into the experimental device respectively, and measure the output rudder angle signal, which is then compared with the command rudder angle signal.

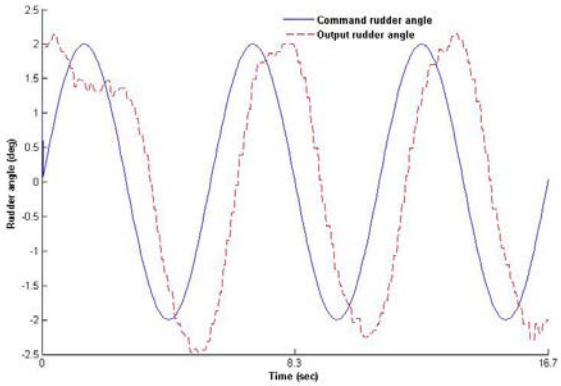

Fig.14. Experimental results of the command sine rudder angle signal with the frequency value of 0.18Hz

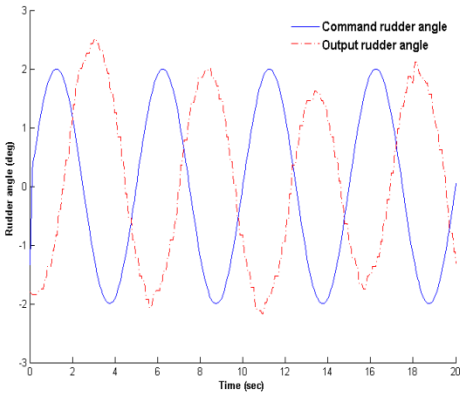

Fig.15. Experimental results of the command sine rudder angle signal with the frequency value of 0.2Hz

As per Fig.14 and 15, the experimental results show that the VSSD's system bandwidth is 0.18Hz, and the overlarge phase lag is the reason why the experimental prototype can't follow with the command rudder angle signal, which is consistent with the results simulated from the nonlinear model.

The linear model can't assess the VSSD's system bandwidth correctly since the factors of the control subsystem are out of consideration, namely the sampling time t_1, t_2, t_3 and the maximum setting changing rate of the motor speed $a_{\max}$. In the linear model, the control subsystem is viewed as a continuous system, of which the sampling time is infinitely short and the maximum speed changing rate is extremely large. Accordingly, the VSSD's system bandwidth of the linear model is the hydraulic transmission subsystem's bandwidth rather than the VSSD's system bandwidth which is determined by both the control subsystem and the hydraulic transmission subsystem.

5. Conclusion

In this paper, the VSSD's nonlinear mathematical model is derived by a full consideration of the nonlinear factors and the simulation model is set up in AMESim software. Then, quantitative analysis of the VSSD's static and dynamic characteristics are evaluated based on the nonlinear model and linear model respectively. Finally, it is verified by experiments that the deduced nonlinear mathematic model can assess the VSSD's actual performance more accurately. The nonlinear modeling method in this paper is flexible and applicable which is of great significance to the design and optimization of the VSSD.

Reference

[1] J. Hu, 2007, "The Theoretical and Testing Research on the Noises-Control Equipments Used in an Electro-Hydraulic Servo System," Master of Engineering, Huazhong University of Science&Technology, Wuhan.
[2] T. Peng, 2003, "Research on Variable Frequency Pump-Control-Motor Speed Governing and Compension Charateristics," Philosophy Doctor, Zhejiang University, Hangzhou.
[3] K. Zhao, 2007, "Study on the New Low Noise Integrated Actuator," Philosophy Doctor, Beijing University of Aeronautics&Astronautics, Beijing.
[4] G. Feng, J. Guo, 2005, "Valveless Electro-Hydraulic Servo System," Journal of Light Industry Machinery(4), pp. 117-119.
[5] Office of Naval Research, 2008, "Electrically Actuated Submarine Control Surfaces," http://www.onr.navy.mil/02/ccr.htm.
[6] E. Bastian, R. Robert, "An Energetic Comparison Between Valveless and Valve Controlled Active Vibration Damping for Off-Road Vehicle," Proc. 6th JFPS International Symposium on Fluid Power, M. Ivantysynova, ed., Tsukuba, pp. 275-283.

[7] I. Masnaori, H. Noriki, "Main Engine Revolution Control for Ship with Direct Drive Volume Control System," Proceedings of ISME, pp. 26-31.
[8] Z.Y. Xing, Y. Zhang, Y. Hou., L. Jia, 2009, "Modeling of Electrohydraulic System and Its Application," Journal of System Simulation(6), pp. 1720-1725.
[9] H.L. Wang, J.G. Cao, 1997, "Development Revolution and Prospect of System Simulation," Journal of System Simulation(9), pp. 1-3.
[10] S. Wang, 2001, "Study on Visual Dynamic Modeling Technique of Hydraulic System and Its Realizing Method in Software," Philosophy Doctor, Dalian University of Science&Technology, Dalian.
[11] J. Lv, 2008, "Direct Drive Volume Control Electro-Hydraulic Servo System Designing and Performance Studying," Master of Engineering, Harbin Institute of Technology, Harbin.
[12] Y. Zang, 2007, "Research on Dynamic and Static Performance of Direct Volume Control Electro-Hydraulic Servo System," Master of Engineering, Harbin Institute of Technology, Harbin.
[13] C. Zhao, C. Ning, C. Pan, 2014, "Study on Direct Drive Control Electro-Hydraulic Servo System," Chinese Hydraulics & Pneumatics(12), pp. 105-107.
[14] C. Zhou, 2009, "Research on Electro-Hydraulic Servo System of Direct Drive Control Shakable Cylinder Steering Gear," Master of Engineering, Harbin Institute of Technology, Harbin.
[15] Y. Fu, H. Qi, 2011, LMS Imagine. Lab AMESim System Modeling and Simulation Tutorial, Beijing University of Aeronautics&Astronautics Press, Beijing.
[16] J.S. Qin, S.L. You, 2004, "Features of AMESim Software and Its Application," Construction Machinery and Equipment(12), pp. 6-8.
[17] J. Chong, X. Wang, F. Li, 1995, "Mathematic Model of the Field-Oriented Control Cycloconverter-Fed Synchronous Machine System," Journal of Tsinghua University(35), pp. 1-8.
[18] Y. Liu, J. Du, Y. Xie, 2014, "Modeling and Simulation of Cages Propulsion Motor Vector Control System Based on Simulink /Gui," Computer Simulation(31), pp. 427-432.
[19] S. Xue, H. Xu, F. Chen, 2014, "Study of the PWM Technology of Multiphase Permanent Magnet Synchronous Motor," Journal of Harbin Institute of Technology(46), pp. 123-128.
[20] W. Yu, D. Li, Y. Huang, 2002, "Analysis of Mathematical Model of Hydraulic Servo System of Submarine Steering Gear," Ship Engineering(4), pp. 38-42.
[21] S. Hu, 2010, Automatic Control Principle, Science Press, Beijing.